ISSN 1547-4771, Physics of Particles and Nuclei Letters, 2012, Vol. 9, No. 1, pp. 29–46. © Pleiades Publishing, Ltd., 2012.

PHYSICS OF ELEMENTARY PARTICLES AND ATOMIC NUCLEI. THEORY

Scalar Top Quarks Production in Polarized Photon–Photon Collisions at ILC[1]

A. Bartl[a], W. Majerotto[b], K. Mönig[c], A. N. Skachkova[b], and N. B. Skachkov[d]

[a] *University of Vienna, Faculty of Physics, Vienna*
[b] *Institute for High Energy Physics (HEPHY Vienna), Vienna*
[c] *DESY, Zeuthen, Germany*
[d] *Joint Institute for Nuclear Research, Dubna*

Received May 30, 2011

Abstract—We study pair production of scalar top quarks (stop, $\tilde{t}_1$) in polarized photon–photon collisions with the subsequent decay of the top squarks into b quarks and charginos $\tilde{t}_1 \to b\tilde{\chi}_1^{\pm}$. We simulate this process by using PYTHIA6.4 for an electron beam energy $2E^e_{\rm beam} = \sqrt{s_{ee}} = 1000$ GeV. The energy spectrum of backscattered photons is generated by CIRCE2 program. A set of criteria for physical variables is proposed which leads to a good separation of stop signal events from top quark pair production, being the main background. These criteria allow us to reconstruct the mass of the top squark, provided that the neutralino mass is known.

DOI: 10.1134/S1547477112010037

INTRODUCTION

The scalar top quark, the bosonic partner of the top quark, is expected to be the lightest colored supersymmetric (SUSY) particle. $\tilde{t}_L$ and $\tilde{t}_R$, the supersymmetric partners of the left-handed and right-handed top quarks, mix and the resulting two mass eigenstates $\tilde{t}_1$ and $\tilde{t}_2$ can have a large mass splitting. It is even possible that the lighter eigenstate $\tilde{t}_1$ could be lighter than the top quark itself [1].

Searches for top squarks were performed at LEP and Tevatron and will continue at the LHC and ILC [2]. At ILC it is planned to have the option of a photon linear collider (PLC), as originally planned for TESLA [3]. This will be achieved by using backscattered photon beams by the Compton scattering of laser photon beams with electron beams [4–10].

It has been stressed that the polarization effects in the interactions of backscattered laser photons [4, 6–10] provide additional opportunities for studying the properties of the produced particles (see also [3] and [2]). In the following we study the reaction

$$\gamma + \gamma \to \tilde{t}_1 + \bar{\tilde{t}}_1. \tag{1}$$

Among the possible $\tilde{t}_1$-decay channels within the MSSM (see [11] for details), we focus on the decay $\tilde{t}_1 \to b\tilde{\chi}_1^{\pm}$ followed by the two-body chargino decay $\tilde{\chi}_1^{\pm} \to \tilde{\chi}_1^0 W^{\pm}$, where one of the W's decays hadronically, $W \to q_i\bar{q}_j$, and the other one leptonically, $W \to \mu\nu_\mu$ [13].[2] The final state of this signal process, shown in Fig. 1a, contains two b quarks and two quarks (originating from the decay of one W boson), a hard muon plus a neutrino (from the decay of the other W) and two neutralinos:

$$\begin{aligned}\gamma\gamma \to \tilde{t}_1\bar{\tilde{t}}_1 \to b\bar{b}\tilde{\chi}_1^+\tilde{\chi}_1^- \to b\bar{b}W^+W^-\tilde{\chi}_1^0\tilde{\chi}_1^0 \\ \to b\bar{b}q_i\bar{q}_j\mu\nu_\mu\tilde{\chi}_1^0\tilde{\chi}_1^0.\end{aligned} \tag{2}$$

The main background process is top quark pair production with the subsequent decay $t \to bW^{\pm}$ (for W's we use the same decay channels as in the stop case):

$$\gamma\gamma \to t\bar{t} \to b\bar{b}W^+W^- \to b\bar{b}q_i\bar{q}_j\mu\nu_\mu. \tag{3}$$

The only difference between the final states of stop and top production (shown in Fig. 1b) is that the stop pair production has two neutralinos which are undetectable. Thus, both processes have the same signature: two b jets, two jets from W decay and a muon. In the following we show that the physical variables constructed out of the final state may allow us to reconstruct the scalar top quark mass. In the present paper we consider only top pair production as background.

[1] The article is published in the original.

[2] The process $e^+e^- \to \tilde{t}_1\bar{\tilde{t}}_1$ with the subsequent decay channels $\tilde{t} \to c\tilde{\chi}^0$ and $\tilde{t}_1 \to b\tilde{\chi}_1^{\pm}$ were considered in [12] and [14, 15], respectively.

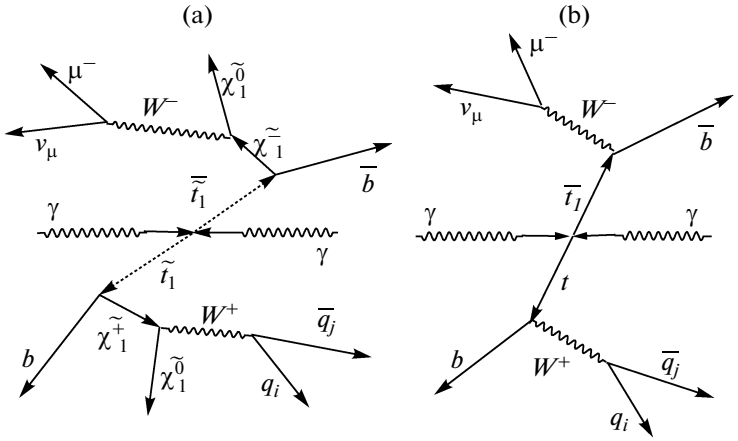

Fig. 1. (a) The stop signal event diagram; (b) the top background diagram.

We analyze the processes (2) and (3) with the help of Monte Carlo samples of the corresponding events. Two programs PYTHIA6.4 [16] and CIRCE2 [17] were used. To simulate stop pair production process (1), we used the PYTHIA6.4 event generator in which the formula for the cross section of the stop pair production in e^+e^- annihilation was replaced by the formula for two scalar particles (s) production $\gamma\gamma \to s\bar{s}$ from [10, 18, 19] (see [20] for the NLO corrections and [21] for more detail about differential cross sections), which takes into account various photon polarization states. The top background was also simulated with PYTHIA6.4. The program CIRCE2 was used to generate the momentum spectra of the backscattered photons involved in the process (1). The energy of the electron beams was chosen to be $E^e_{\text{beam}} = 500$ GeV (i.e., the total e^-e^- energy is $E^{\text{tot}}_{e^-e^-} = \sqrt{s_{ee}} = 1000$ GeV).

We have chosen the mass of stop $M_{\tilde{t}_1} = 167.9$ GeV to be rather close to the mass of the top quark $M_t = (170.9 \pm 1.8)$ GeV [22].[3] Therefore, one expects a rather large contribution from the top background, which means that the choice of this value of the stop mass makes the analysis most difficult. Finding a suitable set of cuts separating stop and top events is therefore crucial.

In Section 1 the important backscattered photon beam characteristics, namely, momentum spectra and luminosity, are considered for the case of polarized photon production in the Compton scattering of polarized laser photons and polarized electrons. The values of the corresponding cross sections are also presented.

In Section 2 we discuss some general characteristics of the signal process $\gamma\gamma \to \tilde{t}_1\bar{\tilde{t}}_1$ and the main background $\gamma\gamma \to t\bar{t}$. Subsection 2.1 includes the kinematical distributions for the produced stop quarks. Subsection 2.2 also deals with the reconstruction of the invariant mass of the two-quark system stemming from the W-bosons decay. Subsection 2.3 contains the kinematical spectra of b quarks. In Subsection 2.4 we demonstrate how to discriminate between the signal muons produced in W-boson decays and those stemming from hadron decays in the same events.

In Section 3 we show the distributions of the global variables as missing energy, total visible (i.e., detectable) energy, the scalar sum of the transverse momenta of all visible particles in the event and the invariant mass of the final-state hadronic jets plus the signal muon. Two further global variables, the invariant mass of all final-state hadronic jets and the missing mass, are also introduced here. It is shown that they are very useful for the separation of background top events.

In Section 4 we propose three cuts which provide a good signal-to-background ratio (S/B).

Section 5 is devoted to the mass reconstruction of the scalar top quark based on the distribution of the invariant mass of one b jet and the other two *non-b* jets (from W decay), provided that the neutralino mass is known.

The final section contains some conclusions.

1. PHOTON BEAM CHARACTERISTICS

Let us mention two main features of photon–photon collisions. The first one is that the monochromaticity of the backscattered photon beam is considerably increased if the mean helicities λ_e and P_c of the electron beam and the laser photon beam are chosen

[3] This value corresponds to the choice of those MSSM parameters (see [14,15] for more detail) which give $M_{\chi_1^+} = 159.2$ GeV and $M_{\chi_1^0} = 80.9$ GeV. Such a parameter point is compatible with all experimental data.

such that $2\lambda_e P_c \approx -1$, as has been shown in [4, 6–10].[4] In this case the relative number of hard photons becomes nearly twice as large in the region of the photon energy fractions $y_i = E_i^\gamma / E_{\rm beam}^e \approx 0.7$–$0.85$, $i = 1, 2$, where $E_{1,2}^\gamma$ are the energies of the two backscattered photon beams. Thereby the luminosity in collisions of these photons increases by a factor of 3–4. The growth of backscatterd photon energy spectra in the region of large y_i with the increase of $(-2\lambda_e P_c)$ is illustrated in Fig. 3 of [7] and in Fig. 2 of [6]. In other words, when $(-\lambda_e P_c)$ increases, the effective "pumping" of soft laser photons into hard backscattered ones increases due to the Compton process. Analogous growth of spectral luminosity $dL_{\gamma\gamma}/dW$ (W is the invariant mass of $\gamma\gamma$ system) in the case that the polarizations in both incoming systems of beam electron and the laser photon satisfy the relation $2\lambda_{1e}P_{1c} = 2\lambda_{2e}P_{2c}$ is demonstrated in Figs. 4 of [7] and [6]. As was mentioned in [6], at $2\lambda_e P_c \approx -1$ the photons with the maximal energy ($y_i \approx 0.7$–0.85) are circular polarized and their helicity is close to $(-P_c)$. Thus, in the limit $2\lambda_{1e}P_{1c} = 2\lambda_{2e}P_{2c} = -1$, the produced pair of most energetic photons have total angular momentum $J = 0$ or $J = 2$, depending on the signs of P_{1c} and P_{2c}. This allows one to measure the cross sections σ_0 and σ_2 which correspond to collisions of $\gamma\gamma$ pairs having total angular momentum 0 or 2, respectively.

The other feature stems from the fact that, unlike the situation at an electron-positron collider, the energy of the beams of backscattered photons will vary from event to event. As already mentioned in the Introduction, we use the program CIRCE2 [17] for the energy spectra of the colliding backscattered photons, as well as the values of photon beam luminosities. CIRCE2 uses as input the data files that were generated for TESLA using the code and the set of beam parameters described in [3, 9, 24].[5] We use as a reasonable approximation the CIRCE2 output spectra obtained on the basis of the above-mentioned data files that were originally generated for $E_{e^-e^-}^{\rm tot} = 800$ GeV and scale them (by 1000/800) to the higher beam energy $2E_{\rm beam}^e = E_{e^-e^-}^{\rm tot} = 1000$ GeV.

The photon energy spectrum obtained in this way without any cuts with CIRCE2 for this total energy $E_{e^-e^-}^{\rm tot} = 1000$ GeV is shown in Fig. 2.[6] Two peaks are clearly seen in this figure. The left one at a low photon energy is caused by the multiple Compton scattering and beamstrahlung photons [3, 9, 24]. The second one, according to [4, 6–10], appears in the region of hard photon production $y_{1,2} \approx 0.83$. It shows the degree of monochromaticity of the produced backscattered high-energy photons.

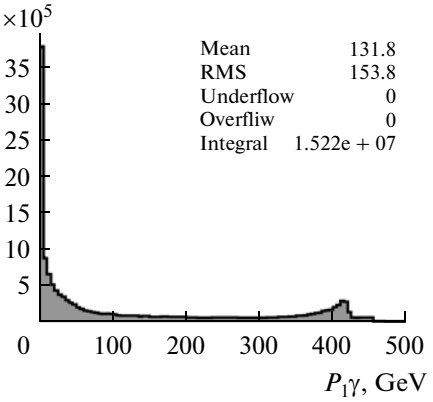

Fig. 2. The whole photon momentum spectrum generated by CIRCE2.

The energy spectra of backscattered photons, as provided by CIRCE2, are used as input for PYTHIA for the generation of stop pair production events. Due to the stop pair mass threshold $2M_{\tilde{t}_1}$, only in about 0.3% of the CIRCE2 events the energy of produced backscattered $\gamma\gamma$ system is high enough for the generation of $\gamma\gamma \to \tilde{t}\tilde{t}$ signal events by PYTHIA.

The correlations between the energies of two colliding photons given by CIRCE2 are shown in the plots a and b of Fig. 3.

The two-dimensional plot a in Fig. 3 shows the correlation between the energy fractions of produced photons y_1 and y_2 for the case that the two colliding backscattered photons have opposite sign helicities, i.e., when the total helicity of $\gamma\gamma$ system $J = 2$.[7] The plot b is for $J = 0$; i.e., it is for the case that the two colliding backscattered photons have the same sign helicities. The distribution in the plot b shows maxima at $y_{1,2} \approx 0.83$, which corresponds to the high-energy peak in Fig. 2 and $2\lambda_e P_c \approx -1$. The number of generated events in the cases a and b are shown by the "Integral" values in the statistic frames of both plots. They were chosen in such a way as to produce equal number (50000) of events at the PYTHIA level of simulation (see "Integral" values in the plots c and d) of the two different samples of signal stop production events having different polarization states of the incoming $\gamma\gamma$ pairs.

[4] A laser beam polarization of 100% can be assumed. An electron polarization of 85% is expected at the ILC.

[5] The spectra obtained by CIRCE2 are in agreement [25] with the code CAIN [23, 26].

[6] Examples of energy, photon polarization and $\gamma\gamma$ luminosity spectra, obtained for a set of different values of total energy $E_{e^-e^-}^{\rm tot}$, can be seen in [3, 6–9, 27].

[7] See Fig. 2 of [27] as an illustration.

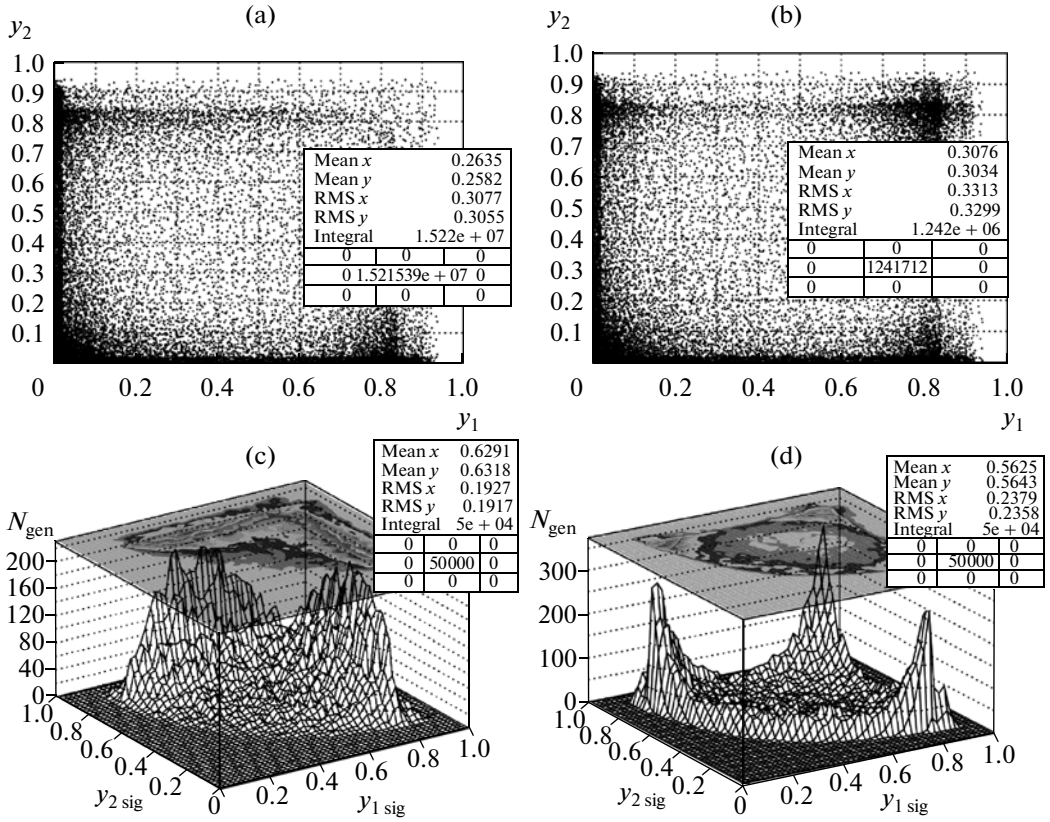

Fig. 3. (a) Correlation spectra of the energy fractions y_1 and y_2 for events generated by CIRCE2 for the case of the opposite sign polarizations of backscattered photons ("$J = 2$ case"). (c) Correlation spectrum for that part of the events shown in plot a in which the energy of $\gamma\gamma$ system is above the threshold of stop pair production. Plots (b) and (d) are the same correlation spectra as (a) and (c) spectra but obtained for the case of the same sign polarizations of backscattered photons ("$J = 0$ case"). $E^{\mathrm{tot}}_{e^-e^-} = 1000$ GeV.

The lower two plots c and d of Fig. 3 are three-dimensional plots with their projections onto the $y_1 - y_2$ plane. They also show the correlations between the energy fractions y_1 and y_2 of the backscattered photons. In these plots we include only those events that lead to the production of a stop–antistop $\tilde{t}\tilde{t}$ pair. The left side of Fig. 3 shows the plots for the opposite sign polarization case (i.e., $J = 2$) and the right side for the same sign polarization case (i.e., $J = 0$). The plots b and d show the enhancement of the $J = 0$state contribution at $y_{1,2} \approx 0.83$.

It is worth mentioning that in a real photon–photon collision experiment none of these cases would appear in a pure form because of the unavoidable presence of some admixture of other photon polarization states.[8]

The simultaneous change of the signs of the laser photon and beam electron helicities at only one side of the colliding beams does not change the equality $2\lambda_{1e}P_{1c} = 2\lambda_{2e}P_{2c}$ [6–10], but leads to a different beam configuration, which may influence the shape of the luminosity spectrum. In Fig. 4 we present the correlation plots that are analogous to those of Fig. 3, but this time they are for the case of the above-mentioned simultaneous sign reversal of the laser photon and electron beam polarizations at one side ($i = 2$, for example) of the colliding beams. It is seen from the plots a and c that this combination gives an increase of the contribution of the two-photon system of total angular momentum $J = 2$.

Finally, we give the values of total photon–photon luminosities and the corresponding values of stop pair production cross sections (for the chosen value of the stop mass) obtained from CIRCE2 and PYTHIA6 for $E^{\mathrm{tot}}_{e^-e^-} = 1000$ GeV for the opposite sign ("+–" and "–+") and the same sign ("++" and "––") backscattered photon helicities:[9]

[8] Partly this is due to the fact that the source electron beams are not 100% polarized.

[9] For simplicity, in the following we shall use the notation "++" and " ––" for the same sign photon helicities case and "+–" and "–+" for the opposite sign helicities case.

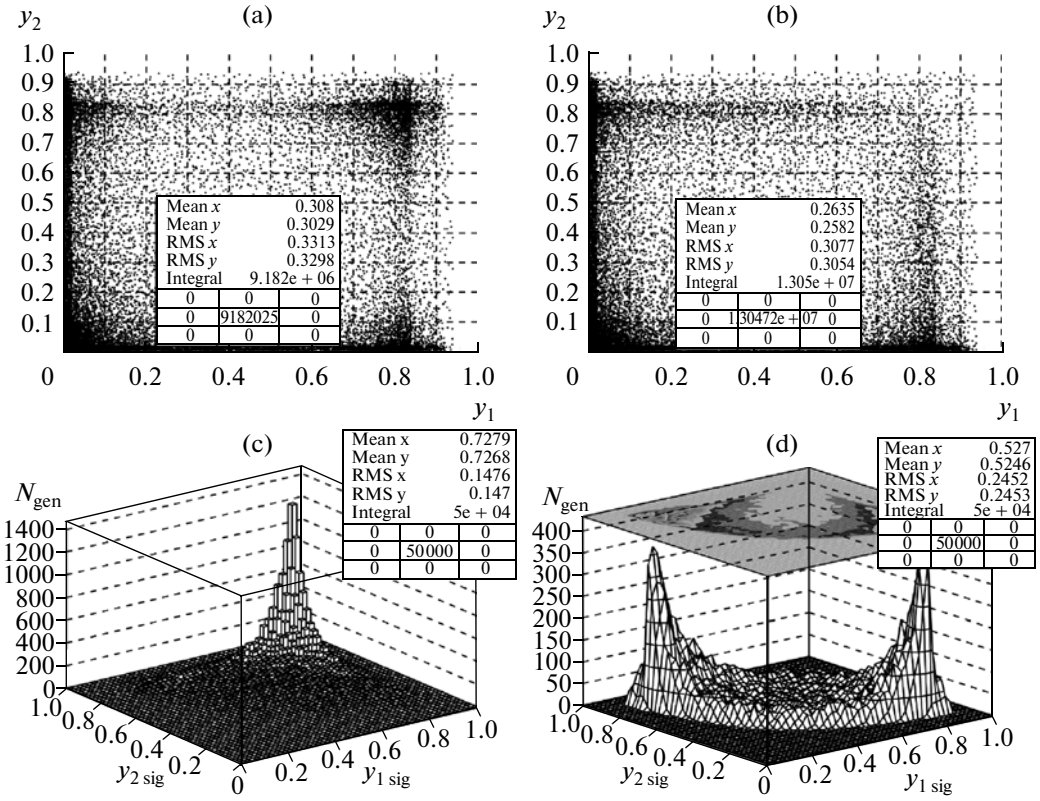

Fig. 4. The same as in Fig. 3 but with the $J=2$ state contribution enhanced.

—for the plots shown in Fig. 3 (i.e., enhanced $J = 0$ state)

$$L^{\gamma\gamma}_{+-\&-+} = 9.35 \times 10^2\,\text{fb}^{-1}\,\text{y}^{-1}; \quad \sigma^{\tilde{t}_1\bar{\tilde{t}}_1} = 2.04\ \text{fb};$$

$$L^{\gamma\gamma}_{++\&--} = 1.02 \times 10^3\,\text{fb}^{-1}\,\text{y}^{-1}; \quad \sigma^{\tilde{t}_1\bar{\tilde{t}}_1} = 3.17\ \text{fb};$$

—for the plots shown in Fig. 4 (i.e., enhanced $J = 2$ state).

$$L^{\gamma\gamma}_{+-\&-+} = 1.02 \times 10^3\,\text{fb}^{-1}\,\text{y}^{-1}; \quad \sigma^{\tilde{t}_1\bar{\tilde{t}}_1} = 3.31\ \text{fb};$$

$$L^{\gamma\gamma}_{++\&--} = 9.35 \times 10^2\,\text{fb}^{-1}\,\text{y}^{-1}; \quad \sigma^{\tilde{t}_1\bar{\tilde{t}}_1} = 4.27\ \text{fb};$$

2. DISTRIBUTIONS OF KINEMATICAL VARIABLES IN STOP AND TOP PRODUCTION

In this section we present various plots for the kinematical distributions of different physical variables based on two samples of 2.5×10^4 stop pair production events generated by CIRCE2 and PYTHIA6.4. They were weighted by the photon–photon luminosity calculated with the help of CIRCE2 and given above for the corresponding polarizations. Analogous plots are also given for 1.0×10^5 generated background top events.

The generation of all events, i.e., for the stop and top production, was done separately for both possible combinations of photon polarizations, i.e., for the same sign ("++" and "− −") and for the opposite sign ("+−" and "−+") helicities.

In the following we present only those plots which correspond to the case that the relative alignment of laser photon and beam electron helicities enhances the contribution of the colliding two-photon system with the total angular momentum $J = 0$ (i.e., corresponding to Fig. 3).[10]

To find the jets, we use the subroutine PYCLUS of PYTHIA. The parameters of this jet finder are chosen such that the number of jets is exactly four. Technically, b jets are defined as jets that contain at least one B hadron. Their decay may be identified by the presence of a secondary vertex [28].

All the figures presented in this paper are obtained after applying the first cut (see Section 4) which superimposes a natural restriction on b jets and allows one to get the samples of events which would be closer to the samples obtained after using all cuts.

2.1. Distributions in Stop Events

Figures 5–8 show some general kinematical distributions characteristic of the produced stop pair system,

[10] The case of $J = 2$ is easier for background suppression due to spin 1/2 of the top quark.

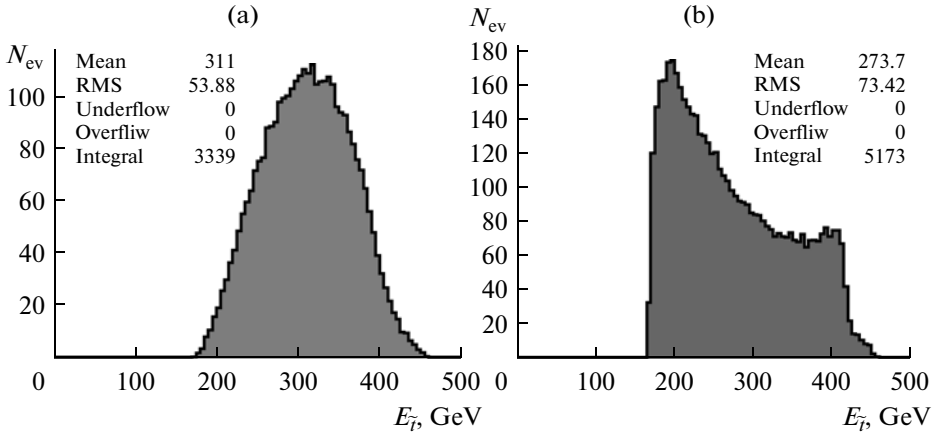

Fig. 5. Stop energy $E_{\tilde{t}_1}$ spectra. (a) "+−" and "−+" polarizations; (b) "++" and "− −" polarizations.

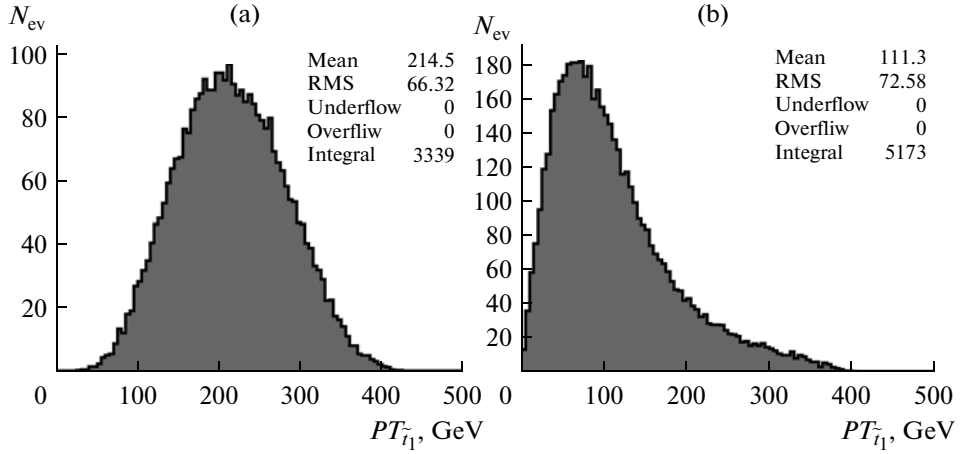

Fig. 6. Stop transverse momentum $PT_{\tilde{t}_1}$ spectra. (a) "+−" and "−+" polarizations; (b) "++" and "− −" polarizations.

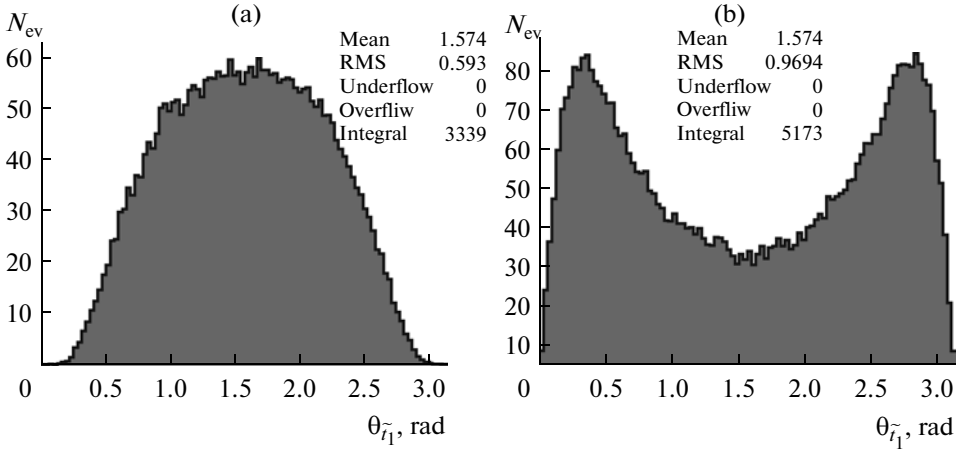

Fig. 7. Stop polar angle $\theta_{\tilde{t}_1}$ spectra. (a) "+−" and "−+" polarizations; (b) "++" and "− −" polarizations.

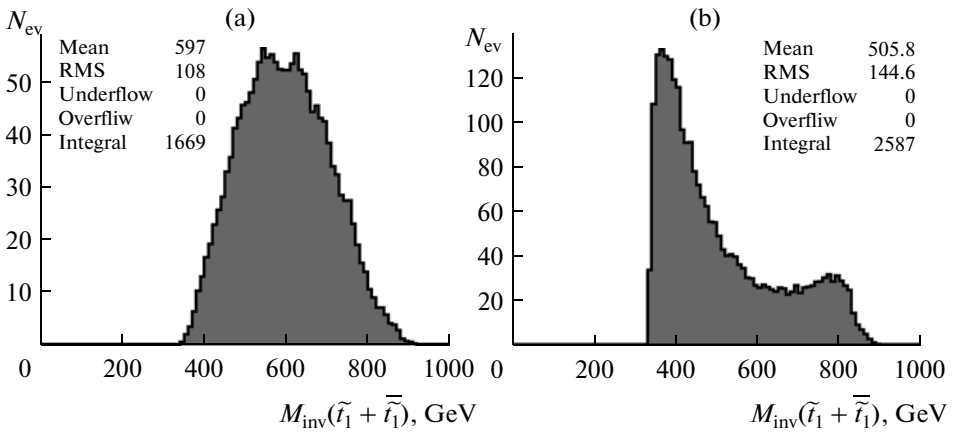

Fig. 8. Stop pair invariant mass $M_{inv}(\tilde{t}_1 + \bar{\tilde{t}}_1)$ spectra. (a) "+−" and "−+" polarizations; (b) "++" and "− −" polarizations.

i.e., the distributions of the energy of the stop or antistop $E_{\tilde{t}_1}$, the transverse momentum $PT_{\tilde{t}_1}$, the polar angle $\theta_{\tilde{t}_1}$ (all in e^-e^- c.m.s.) and the invariant mass of the produced stop pair $M_{inv}(\tilde{t}_1 + \bar{\tilde{t}}_1)$. In these plots we do not distinguish between stop and antistop. By comparing the left-hand side of these figures with the right-hand side, one sees the effects of the different chosen polarizations (and corresponding luminosities).

In Fig. 5 one can see that the stop energy $E_{\tilde{t}_1}$ spectra start close to the value of the chosen stop mass $M_{\tilde{t}_1} = 167.9$ GeV. In the case of opposite sign photon polarizations (plot a) the spectrum has a peak at $E_{\tilde{t}_1} \approx 320$ GeV and it is characterized by a high mean value $E_{\tilde{t}_1}^{mean} = 311$ GeV. It means that the produced stops are rather energetic. In the case of the same sign polarizations (plot b) the energy spectrum is softer, having the main peak at $E_{\tilde{t}_1} = 200$ GeV and the mean value about 274 GeV. So, one may expect that the stops produced in the same sign case are on the average less energetic than in the opposite sign case. One can also see a second smaller peak at $E_{\tilde{t}_1} \approx 400$. This is due to the effect of the luminosity and cross section enhancement in the $J = 0$ case at $y_1 \approx y_2 \approx 0.83$ (see the right-hand plots of Fig. 3).

Figure 6 shows analogous distributions for the stop transverse momentum $PT_{\tilde{t}_1}$. The $PT_{\tilde{t}_1}$ spectrum for the same sign polarizations (plot b) is much softer than for the opposite sign polarizations (plot a), with mean values of 111 and 214 GeV, respectively.

The polar angle $\theta_{\tilde{t}_1}$ distributions are shown in Fig. 7. One can see that the distribution for "+−" and "−+" polarizations (plot a) is very different from that for "++" and "− −" polarizations (plot b).

The invariant mass $M_{inv}(\tilde{t}_1 + \bar{\tilde{t}}_1)$ spectra of the produced stop–antistop system are shown in Fig. 8. For "+−" and "−+" polarizations (plot a) it has a peak around 550 GeV, which is about 170 GeV higher than the analogous peak at 380 GeV for "++" and " −−" polarizations (plot b). Note that the shapes of the distributions of the invariant mass of the stop pairs shown in Fig. 8 follow the energy spectra given in Fig. 5. Thus, the second peak in plot b of Fig. 8 at $M_{inv}(\tilde{t}_1 + \bar{\tilde{t}}_1) \approx 800$ GeV has the same origin as the peak in the plot b of Fig. 5 at $E_{\tilde{t}_1} \approx 400$ GeV.

The vertical axis in the plots shows the number of stops and antistops produced per year ($=10^7$ s) in each bin. Taking the integral of the distributions and dividing its value by two (there is one stop–antistop pair in each event), one can get the total number of events expected per year for the applied cuts. These numbers are shown as "Integral" values within the statistical frames in the upper corners of the plots. They are calculated by taking into account the ratio of the photon–photon luminosity in the energy region above the stop pair threshold over the total photon–photon luminosity. In the case of "+−" and "−+" polarizations this ratio is approximately 0.419. From Fig. 8 it is seen that the number of events per year for the "++" and "− −" backscattered photon polarizations is equal to $N_{++/--} = 2587$. It is appreciably larger than the corresponding number of events per year $N_{+-/-+} = 1669$ for "+−" and "−+" polarizations.

2.2. Quark Distributions from W Decay

According to the decay chain (2), the final state has to contain two jets due to the decay of one W boson into two quarks $W \to q_i + \bar{q}_j$ (see Fig. 1).

Figure 9 shows the distributions of the energy $E_{W\text{-quark}}$ of the quarks produced in the W-boson decay

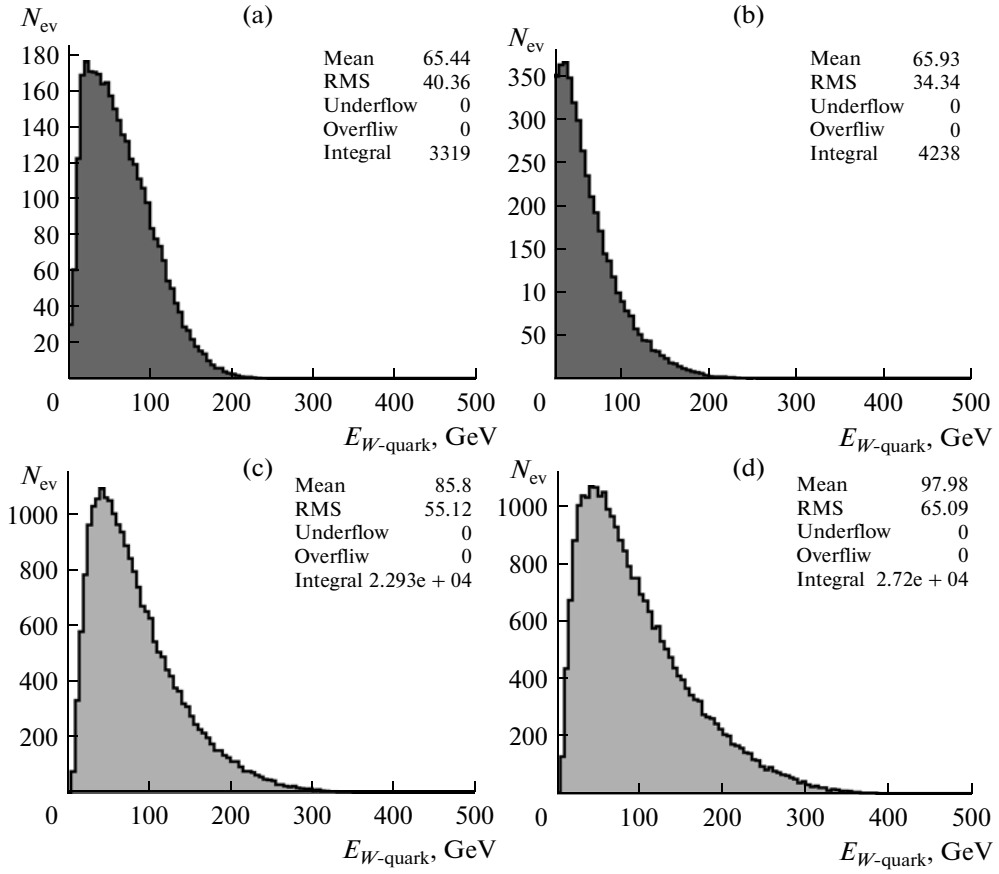

Fig. 9. Energy spectra of the quarks from W-boson decay. The plots (a) and (b) are for the stop pair production; the plots (c) and (d) are for the top pair production. (a, c) "+−" and "−+" polarizations; (b, d) "++" and "− −" polarizations.

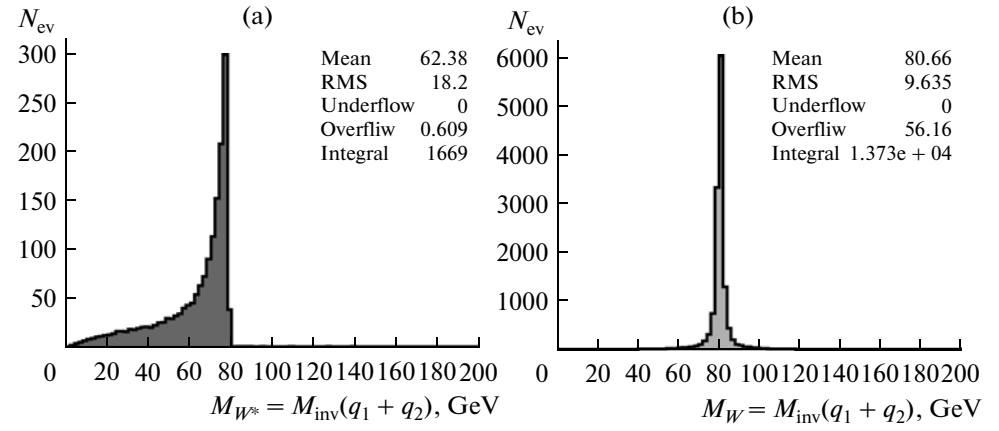

Fig. 10. The invariant mass of two quarks $M_W = M_{inv}$ (quark1 + quark2), reconstructed from the vectorial sum of 4-momenta of two quarks that are produced in $W \to q_i + \bar{q}_j$ decay. (a) Stop pair production; (b) top pair production.

(which we call "W quarks") for stop (plots a and b) and top (plots c and d) production. The plots a and c present "+−" and "−+" polarizations, while the plots b and d present "++" and "− −" polarizations. The stop-quark spectra begin at zero and go up to 220 GeV, with a mean value of ≈65 GeV, while the top-quark spectra go up to approximately 300–350 GeV, with mean values of 85–97 GeV.

Figure 10 shows the spectrum of the invariant mass $M_W = M_{inv}$ (quark1 + quark2) reconstructed from the vectorial sum of 4-momenta of the two "W quarks". The main features of these plots practically do not dif-

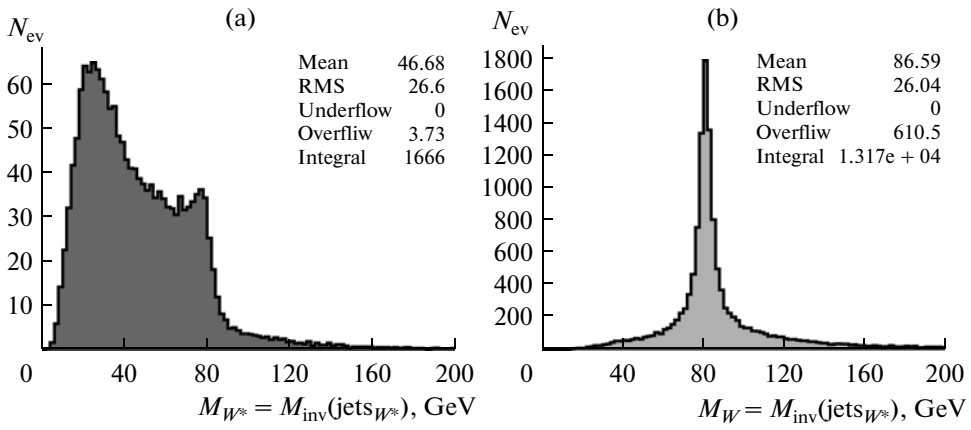

Fig. 11. Number of generated events versus the reconstructed invariant mass of "all-*non-b* jets". (a) Stop pair production; (b) Stop pair production.

fer for "+−" and "−+" and the "++" and "—" polarization cases. Therefore, we do not show them separately. The plot a is for stop pair production, the plot b is for top production. In the plot a of Fig. 10 one clearly sees the virtual nature of the W boson in the stop pair production case. Hence, in the stop case the invariant mass of two quarks produced in the decay of the virtual W boson (W^*) is smaller than the mass of a real W boson. In top production (see the plot b of Fig. 10) there is a peak in the invariant mass distribution at the mass value of the real W boson.

Figure 11 shows the corresponding plots at the jet level. The invariant mass is built of "all-*non-b* jets" (or, shortly, "$jets_{W^*}$"). One can see from the plot a that in the stop case the peak position of M_{inv} ($jets_{W^*}$) is shifted to the left and a long tail for higher invariant masses appears. As seen from the plot b, in the top case at the jet level the position of the W peak remains at the same value of M_W (with a high precision) as in the plot b of Fig. 10, except some shifting of the mean value. From comparison of the plots a and b of Fig. 11 we conclude that the cut M_{inv} ($jets_W$) ≤ 70 GeV may allow us to eliminate this tail and a big amount of the top background. The comparison of the plots b of Figs. 10 and 11 provides the information about the effect of quark to jet fragmentation.

2.3. b-Quark and b-Jet Distributions in Stop and Top Production

In the case of stop decay into a b quark and a chargino, $\tilde{t}_1 \to b\tilde{\chi}_1^{\pm}$, the jets produced in b-quark hadronization are observable objects.

In Fig. 12 we show in the plots a and b the distributions of the energies E_b of the b and $\bar{b}$ quarks (which we do not distinguish in the following) produced in the decay $\tilde{t}_1 \to b\tilde{\chi}_1^{\pm}$ for the "+−", "−+" and "++", "−−" polarizations, respectively. Both spectra begin at $E_b \approx$ 4 GeV, corresponding to the b-quark mass, and go up to $E_b \approx 34$ GeV. The mean values are about 14 and 13 GeV, respectively. The plots c and d of Fig. 12 are two analogous plots for top pair production. The corresponding spectrum in top production is much harder and its main part is concentrated within the interval $45 < E_b < 150$ GeV. The mean values are $E_b \approx$ 113 GeV and $E_b \approx 130$ GeV, respectively, which is almost four times higher than the end point of the b-jet energy spectra in the stop events. Comparing the distributions a and b in Fig. 12 with the corresponding ones in Fig. 5, one can conclude that in stop pair production the b quark takes only a smaller part of the parent stops energy than the b quark gets in the background top case.

The b quarks produced in top decays are very energetic. Most of the top events have $E_b \geq 25$ GeV and $PT_b \geq 20$ GeV. The difference from stop decay is easily understandable. The stop decays into a heavy chargino, whereas the top decays into a real W boson whose mass is only half of the mass of the chargino $M_{\chi_1^{\pm}}$. Therefore, the b quarks in top decays have a larger phase space than the b quarks in stop decays.

2.4. Distributions of the Signal Muons

To select the signal stop pair production events (see Fig. 1a), one has to identify the muon from the W decay. There are, however, also muons in the event coming from leptonic and semileptonic decays of hadrons. Figures 13a and 13b show, respectively, the energy distribution of the signal muons $E_{sig\text{-}mu}$ and the energy spectra $E_{dec\text{-}mu}$ of the muons stemming from hadron decays (both for the case of the same polarization) within the detector volume, for which we took the size parameters from [2]. It can be seen from Fig. 13b that the decay muons have a rather small energy $E_{dec\text{-}mu}$. Their mean value is about 0.85 GeV. The analogous spectra for the signal muons in Fig. 13a

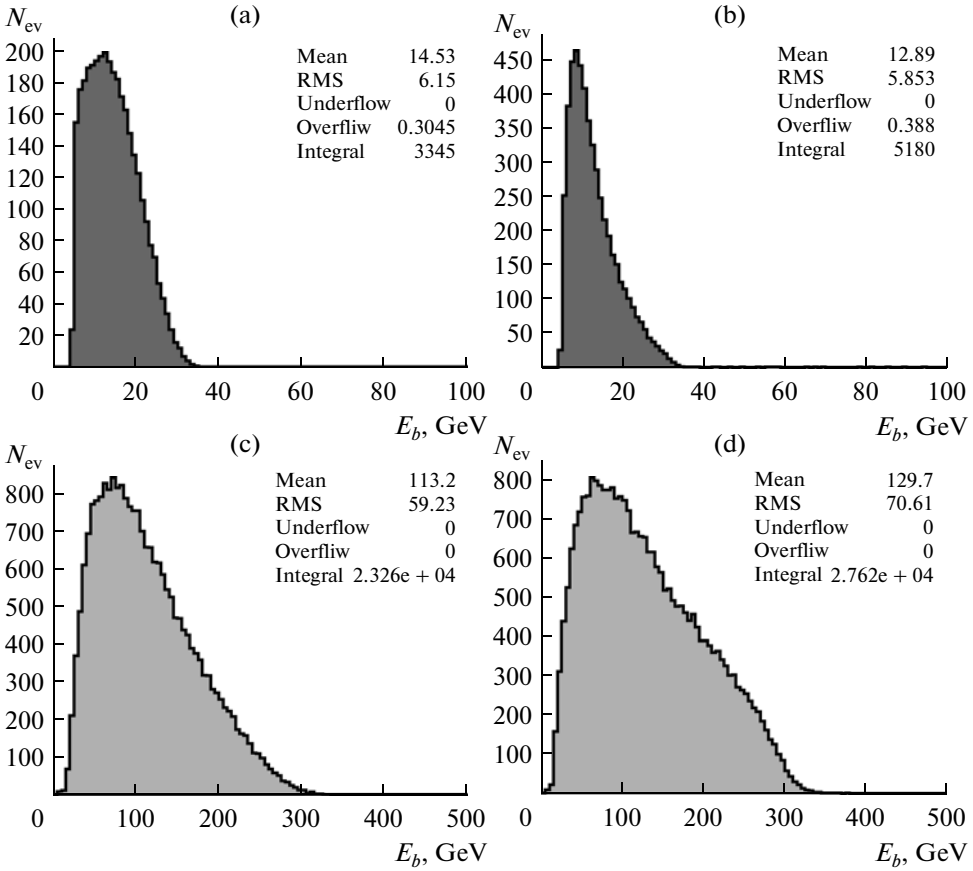

Fig. 12. b- and $\bar{b}$ -quark energy spectra. The plots (a) and (b) are for the stop pair production; the plots (c) and (d) are for the top pair production. (a, c) "+−" and "−+" polarizations; (b, d) "++" and "− −" polarizations.

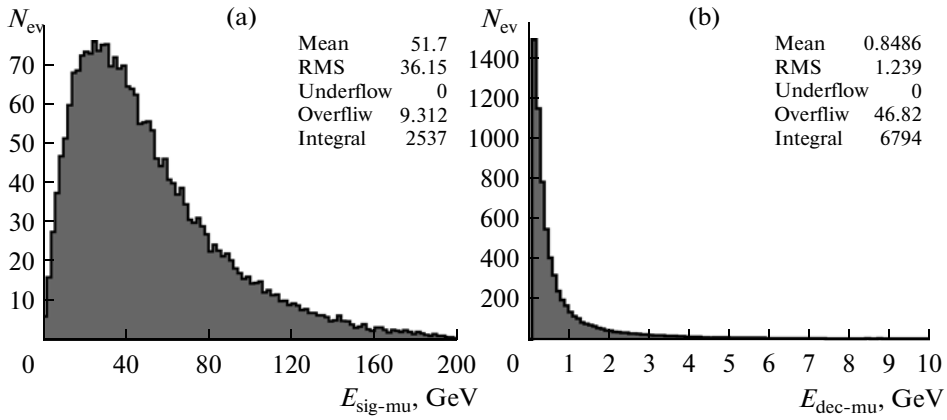

Fig. 13. Energy distributions of muons from stop decays (a) and from leptonic and semileptonic decays (b).

show that the signal muons have a much higher energy $E_{\text{sig-mu}}$ and transverse momentum $PT_{\text{sig-mu}}$. The mean value of the signal muons energy $E^{\text{mean}}_{\text{sig-mu}} = 51.7$ GeV is about 60 times higher than the mean value of the energy of the decay muons. Therefore, one can cut off most low-energy decay muons rejecting those with $E_{\text{mu}} \le 6$ GeV. Such a cut leads to a loss of about 2% of signal events, as seen from Fig. 13 (the bin width in this plot is 2 GeV).

We have also studied another way to select the signal muon from W decay. If the axes of all four jets in the event are known, then in general the signal muon has the largest transverse momentum with respect to any of these jet axes.

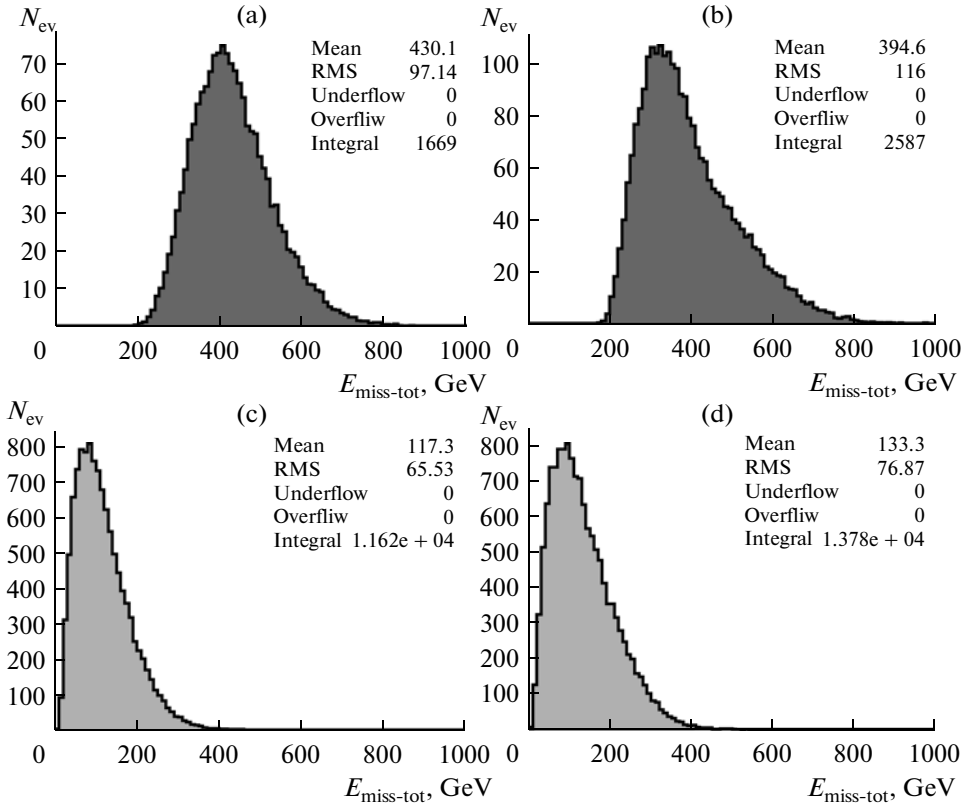

Fig. 14. Missing energy $E_{\text{miss-tot}}$ distribution. The plots (a) and (b) are for stop pair production; the plots (c) and (d) are for top pair production. (a, c) "+−" and "−+" polarizations; (b, d) "++" and "− −" polarizations.

3. SOME GLOBAL VARIABLES

In stop pair production the two neutralinos and the energetic neutrino from the W-boson decay escape detection. The simulation with PYTHIA6 allows us to estimate the missing energy and the missing transverse momenta that are carried away by these particles. We also take into account the non-instrumented region around the beam pipe given by the polar angle intervals $\theta < 7^\circ$ and $\theta > 173^\circ$.

The distributions of the total missing energy for stop production and top production are presented in the upper and lower plots of Fig. 14, respectively. In stop pair production (see the plots a and b), the $E_{\text{miss-tot}}$ spectrum starts at 180–200 GeV (i.e., a bit higher than $2M_{\chi_1^0}$) and it ends at 800 GeV. In top pair production (plots c and d), where the two neutralinos are not present, the missing energy $E_{\text{miss-tot}}$ is much smaller. It starts from ≈10 GeV and finishes at ≈380–420 GeV.

Figure 15 shows the distributions of the total visible energy in event $E_{\text{vis-tot}}$ in stop production (plots a and b) and in top production (plots c and d). The large missing energy in stop production (Fig. 14) is related to the low visible energy (Fig. 15), while in top production the low missing energy correlates with the large visible energy. A cut on the total visible energy of approximately $E_{\text{vis-tot}} < 250$ GeV[11] would eliminate most of the top background, while approximately 10% of the signal events are lost.

An even more efficient separation of the signal and the background can be obtained by using the invariant mass M_{inv} (All jets) of the system that contains all jets (P^i_{jet} is the 4-momentum of the ith jet, $i = 1, 2, 3, 4$):

$$M_{\text{inv}}(\text{All jets}) = \sqrt{\left(\sum_{i=1}^{N\text{jet}} P^i_{\text{jet}}\right)^2}. \quad (4)$$

The corresponding distributions for the signal stop events (upper plots) and for the background top events (lower plots) are shown in Fig. 16. It is seen that the application of the cut M_{inv} (All jets) ≤ 180 GeV leads to a practically complete separation of signal stop and top background events.

4. CUTS AND SIGNAL-TO-BACKGROUND RATIO

To diminish the influence of the jet energy redistribution effect, discussed in [14] and [15], we shall use

[11] That is equivalent to setting a lower limit for the missing energy.

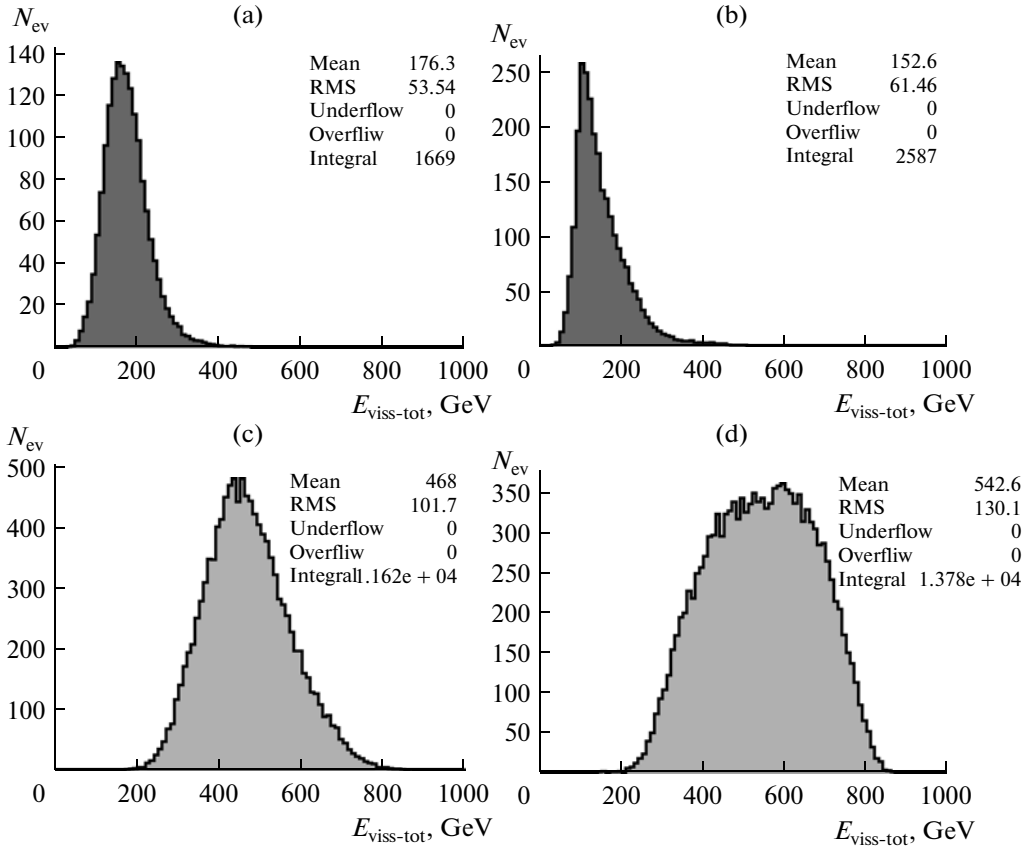

Fig. 15. Total energy $E_{\text{vis-tot}}$ distribution. The plots (a) and (b) are for stop pair production; the plots (c) and (d) are for top pair production. (a, c) "+−" and "−+" polarizations; (b, d) "++" and "− −" polarizations.

the cuts considered above for the $E_{\text{vis-tot}}$ and M_{inv} (All jets). These variables, by deinition, include the total 4-momentum of all jets, deined as the vectorial sum of the 4-momenta of all jets. Therefore, they do not suffer from energy redistribution between jets. Based on our above results, we will use the following three cuts to separate the signal and background events:

—there must be at least two b jets in an event:

$$N_{b\text{-jets}} \geq 2; \quad (5)$$

—the invariant mass of all jets must be less than 180 GeV:

$$M_{\text{inv}}\,(\text{All jets}) \leq 180\ \text{GeV}; \quad (6)$$

—the detected energy $E_{\text{vis-tot}}$ must be less than 250 GeV:

$$E_{\text{vis-tot}} \leq 250\ \text{GeV}. \quad (7)$$

As was mentioned in Section 2, the figures presented in this paper are obtained after applying the first cut in order to get the right picture of jets when the b jets are clearly determined. Before this cut the numbers of signal stop events (per year) were: 1903 in the case of "+−" and "−+" polarizations and 3233 in the case of "++" and "− −" polarizations.

These three cuts for the case with $J = 0$ enhanced state considered here improve the signal-to-background ratio in the case of "+−" and "−+" polarizations from $S/B = 0.15$ to $S/B \approx 60$, losing about 23.7% (from 1903 $\rightarrow$ 1453) of the signal stop events and reduction of background top events from 1.227×10^4 to 24. In the case of "++" and "− −" polarizations an improvement of the signal-to-background ratio is from $S/B = 0.222$ to $S/B \approx 123$, with a loss about 27.7% (from 3233 to 2338) of the signal stop events and a reduction of the background top events from 1.441×10^4 to 19 (per year).

Finally, we present the efficiency values for the three cuts (5)–(7). We define them as the summary efficiencies. It means that if ε_1 is the efficiency of the first cut (5), ε_{12} is the efficiency of applying the first cut (5) and then the second cut (6). Analogously, ε_{123} is the efficiency of the successive application of the cuts (5), (6) and (7).

For signal stop events:

"+−" and "−+" polarizations: $\varepsilon_1 = 0.88$; $\varepsilon_{12} = 0.78$; $\varepsilon_{123} = 0.76$;

"++" and "− −" polarizations: $\varepsilon_1 = 0.80$; $\varepsilon_{12} = 0.73$; $\varepsilon_{123} = 0.72$;

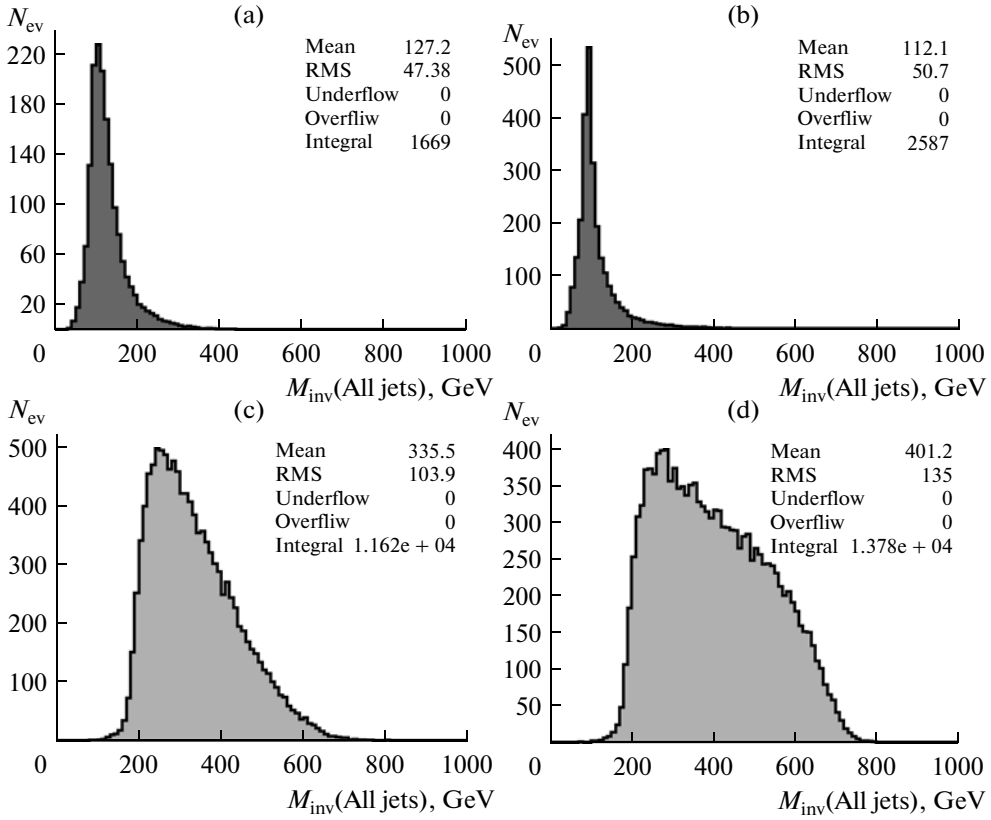

Fig. 16. Distribution of number of events versus the reconstructed invariant mass of all jets M_{inv} (All jets). The plots (a) and (b) are for stop pair production; the plots (c) and (d) are for top pair production. (a, c) "+−" and "−+" polarizations; (b, d) "++" and "− −" polarizations.

For background top events:

"+−" and "−+" polarizations: $\varepsilon_1 = 0.94$; $\varepsilon_{12} = 0.011$; $\varepsilon_{123} = 0.002$;

"++" and "− −" polarizations: $\varepsilon_1 = 0.94$; $\varepsilon_{12} = 0.007$; $\varepsilon_{123} = 0.001$.

5. DETERMINATION OF THE SCALAR TOP QUARK MASS

Another variable of interest is the invariant mass M_{inv} (b jet, Jets$_W$):

$$M_{\text{inv}}(b \text{ jet}, \text{Jets}_W) \equiv \sqrt{(P_{b\text{-jet}} + P_{\text{Jets}_W})^2}, \qquad (8)$$

which is constructed as the modulus of the vectorial sum of the 4-momentum $P_{b\text{-jet}}$ of the b jet, plus the total 4-momentum of Jets$_W$ system, i.e., *non-b* jets stemming from the W decay ($P_{\text{Jets}_W} = P_{\text{jet1}_W} + P_{\text{jet2}_W}$, as there are only two jets allowed to be produced in W decay). More precisely, if the signal event contains a μ^- as the signal muon (see Fig. 1), we have to take the b jet ($\bar{b}$ jet in the case of μ^+ as the signal muon). This is only possible if one can discriminate between the b and $\bar{b}$ jets experimentally. Methods of experimental determination of the charge of the b jet ($\bar{b}$ jet) were developed in [29]. In this paper we do not use any b-tagging procedure. The PYTHIA information about quark flavor is taken for choosing the b and $\bar{b}$ jets. In reality, according to [29], a 50% efficiency of the separation of b jets and 80% of the corresponding purity can be expected.

The distributions of the invariant masses of the "b jet + Jets$_W$" system in the case of stop pair production are shown in the plots a and b of Fig. 17 for the two polarization combinations, as well as in the case of top pair production in the plots c and d. Their analogs M_{inv} (b, 2 quarks$_W$), obtained at quark level, are presented in Fig. 18. The distributions shown in both figures were obtained without use of cuts (6) and (7).

In the top case the invariant mass M_{inv} (b, 2 quarks$_W$) of the system composed of a b quark and two quarks from W decay should reproduce the mass of their parent top quark (see Fig. 1). The distributions of events $dN^{\text{event}}/dM_{\text{inv}}/5$ GeV expected in each bin of 5 GeV versus the invariant mass $M_{\text{inv}}(b, 2 \text{ quarks}_W)$ of the parent three quarks as well as the invariant mass of jets produced by these quarks, i.e., $M_{\text{inv}}(b \text{ jet}, \text{Jets}_W)$, are

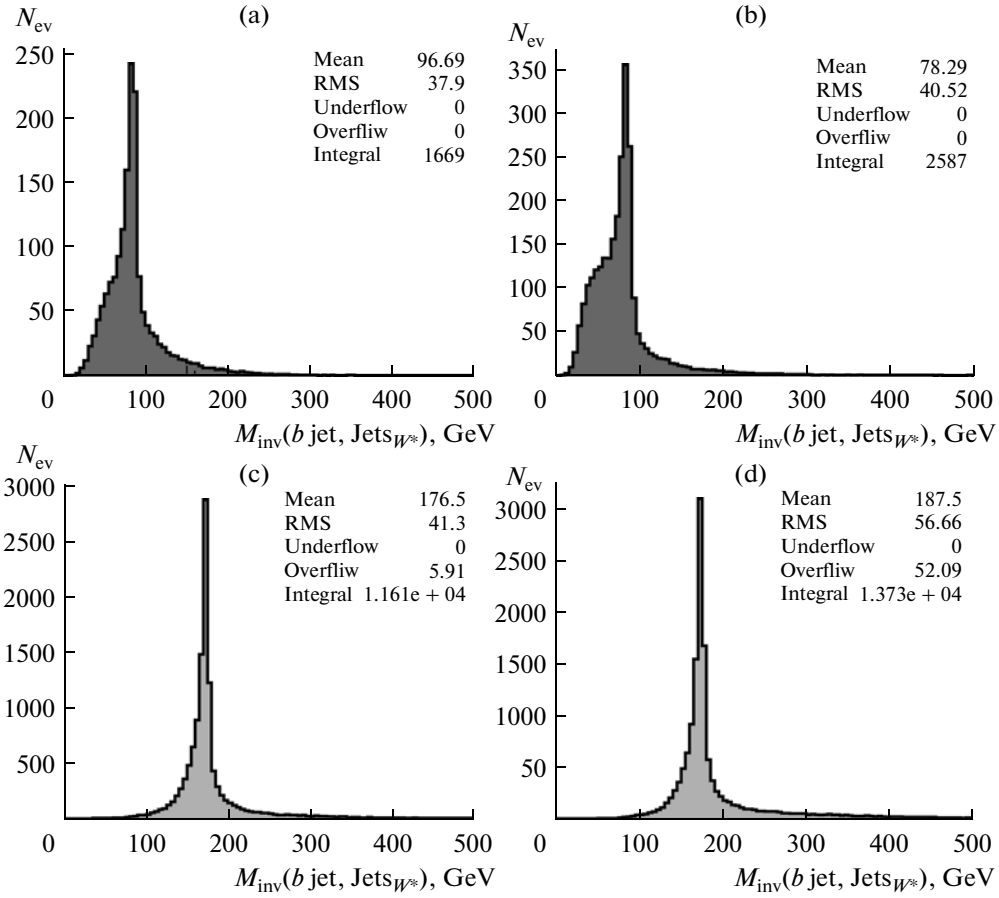

Fig. 17. The spectra of the invariant masses M_{inv} (b jet, Jets$_W$) obtained without use of cuts (6) and (7). Plots (a) and (b) are for stop pair production; plots (c) and (d) are for top pair production. (a, c) "+−" and "−+" polarizations; (b, d) "++" and "− −" polarizations.

shown for jet and quark levels in the plots c and d of Figs. 17 and 18, respectively, for both polarizations. These distributions have an important common feature. Namely, they show that the peak positions at jet level and at quark level, practically coincide to a good accuracy with each other as well as with the input value of the top quark mass $M_{\text{top}} = 170.9(\pm 1.8)$ GeV. It is also seen from Fig. 17 that the quark hadronization into jets leads to a broadening of very small tails which are seen in the invariant mass distribution at quark level (Fig. 18). The right tails, which appeared at jet level (see Fig. 17), are a bit lower than the left tails and are longer than the left ones. One may say that the peak shape at jet level still looks more or less symmetric. The main message from these plots is that the appearance of tails due to quark fragmentation into jets does not change the position of the peak, which allows us to reconstruct the input top mass both at quark and jet levels.

An analogous stability of the peak position at the jet and quark levels for the stop case can be seen in the plots a and b of Figs. 17 and 18. Note that, according to the stop decay chain (2), the right edge of the peak of the invariant mass distribution of the "b + 2 quarks$_W$" system corresponds to the mass difference $M_{\tilde{t}_1} - M_{\tilde{\chi}_1^0}$.

The distributions of the invariant mass of the "b + 2 quarks$_W$" system (plots a and b) and of the invariant mass of the "b jet + Jets$_W$" system in the case of stop pair production are shown in Fig. 19. Thereby only those stop events are taken that pass the cuts (5)–(7).

Let us recall that according to Section 4 the application of the cuts (5)–(7) leaves only 1924 background top events (respectively, for "++", "− −" and "+−", "−+" combinations of photon polarizations) and saves about 76.3% of signal stop events. It means that the distributions shown in the plots c and d of Fig. 17 would change drastically and resemble a random distribution of the 19–24 top events in a rather wide interval. The corresponding plots c and d of top production events which pass the cuts (5)–(7) are made with a much larger simulated statistics and are shown in Fig. 20. One sees that the surviving background top events will be mostly distributed in the region $30 \le M_{\text{inv}}$ (b jet, Jets$_W$) ≤ 180 GeV. This region is by about thirty times wider than the 5 GeV width of the peak intervals

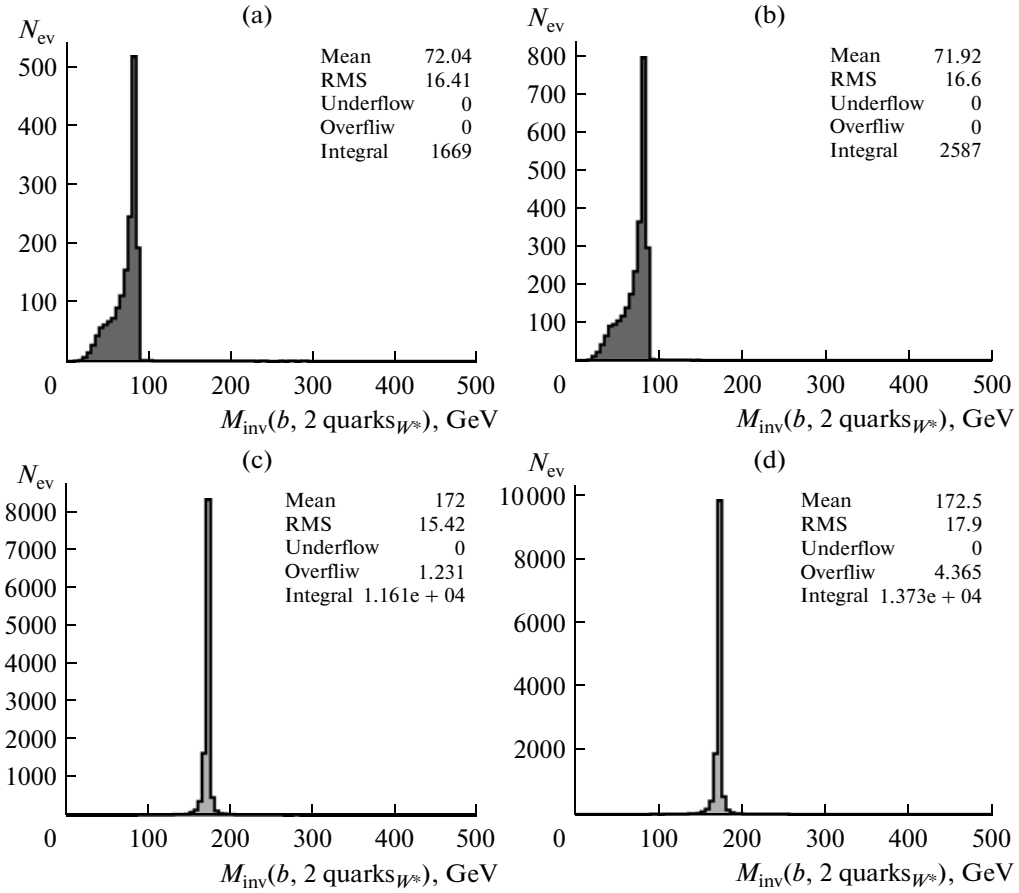

Fig. 18. The spectra of the invariant masses M_{inv} (b, 2 quarks$_W$) obtained without use of cuts (6) and (7). Plots (a) and (b) are for stop pair production; plots (c) and (d) are for top pair production. (a, c) "+−" and "−+" polarizations; (b, d) "++" and "− −" polarizations.

in the M_{inv} (b jet, Jets$_W$) distributions which are shown in the stop plots c and d of Fig. 19 (at jet level) and which contain about 230 (for "+−" and "−+" polarizations) and 350 (for "++" and "− −" polarizations) signal stop events left after the cuts. Based on the shape of the distributions shown in the plots c and d of Fig. 20, we can expect that in future measurements the contribution of these 24–19 remaining top background events will not influence the position of the peak of the M_{inv} (b jet, Jets$_W$) distributions (shown in the plots c and d of Fig. 19) which allow one to reconstruct the input value of the stop mass at jet level by adding the mass of the neutralino.

It is seen that the peak positions of the stop distribution at jet level M_{inv} (b jet, Jets$_{W^*}$), obtained after the cuts (5)–(7) (plots c and d of Fig. 19), coincide with the peak positions at quark level (plots a and b of Fig. 19) as well as with the peak positions in the plots a and b of Figs. 17 and 18 obtained without cuts (6) and (7). Let us note that the observed stability of the peak position in both of Figs. 17a, 17b and 19c, 19d is due to the rather moderate loss of the number of events in the peak region (this loss is about 200–250 events per year) after cuts. The cuts lead (as can be seen by comparing the mentioned plots) to a reduction of the right-hand side tails of M_{inv} (b jet, Jets$_{W^*}$) distributions.[12]

Some additional remarks about the tails in the stop distributions are in order now. The origin of the right and left tails of the distributions, shown in the plots a and b of Fig. 19, can be clarified by the results of the stop mass reconstruction by calculating its invariant mass at quark level $M_{inv}(b, 2\ quarks_{W^*}, \tilde{\chi}_1^0)$ as the modulus of the sum of the 4-momenta of all three quarks and the neutralino (see Fig. 1) in stop decay. These results are given in the plots a and b of Fig. 21 which shows a very precise reconstruction of the input stop mass at quark level within the 5 GeV width of the bin containing the peak. Comparing the

[12] The interval 150–350 GeV in Fig. 19b can be used to calculate the width between the grid dots in this plot. It is found to be about 7.4 GeV. This number allows us to estimate the position of the right edge of the peak of the M_{inv}(b jet, Jets$_{W^*}$) distribution, which seems to be shifted to the left side from 100 GeV by a distance which is about two dot intervals, i.e., by less than 14.8 GeV. Thus, we can estimate that the right edge of the peak of the M_{inv}(b jet, Jets$_{W^*}$) distribution lies a little higher than 85.2 GeV.

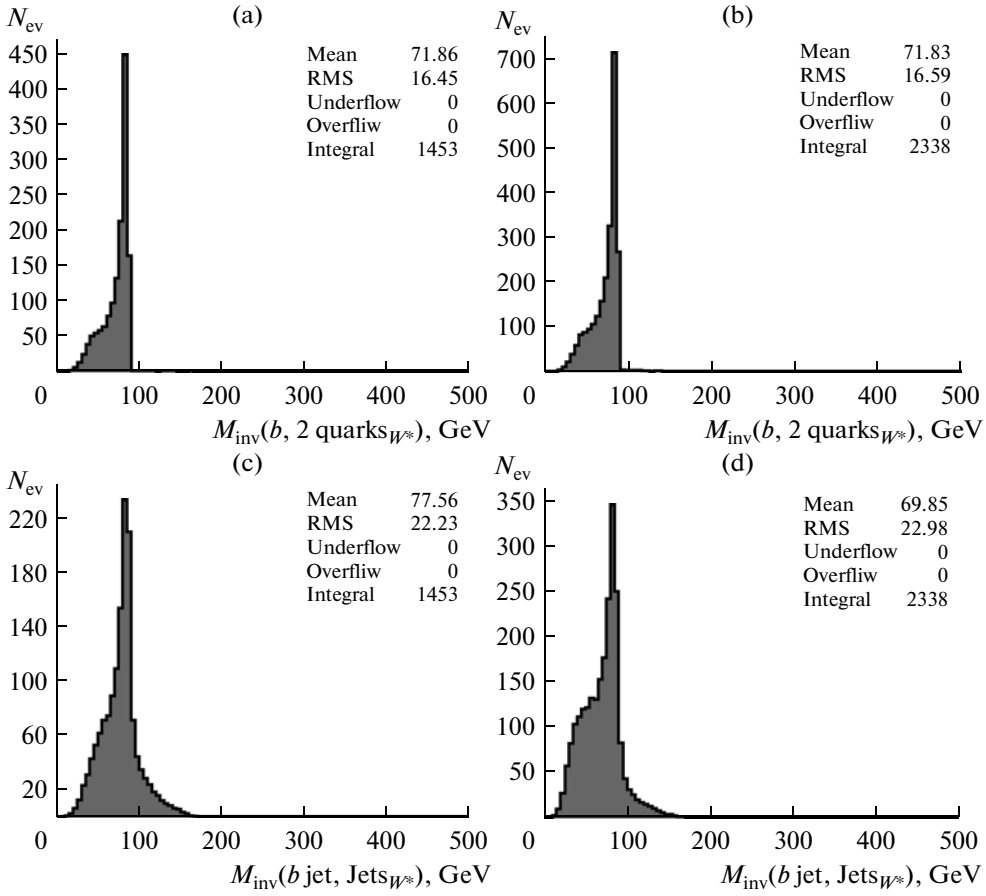

Fig. 19. The spectra of the stop invariant masses after the cuts (14)–(16): Plots (a) and (b) —M_{inv} (b, 2 quarks$_{W^*}$); plots (c) and (d)—M_{inv} (b jet, Jets$_{W^*}$). (a, c) "+–" and "–+" polarizations; (b, d) "++" and "– –" polarizations.

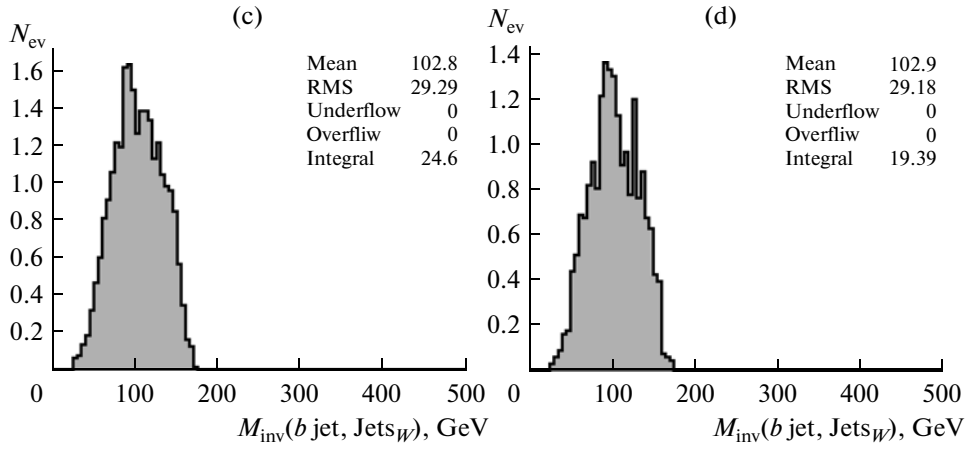

Fig. 20. The spectra of the invariant mass M_{inv} (b, 2 quarks$_W$) for top pair production events after the cuts (5)–(7). (a) "+–" and "–+" polarizations; (b) "++" and "– –" polarizations.

plots a and b of Fig. 19 with the plots a and b of Fig. 21, one can conclude that at quark level the long left tail, as well as the very small right tail, in the distribution of $M_{inv}(b, 2\ quarks_{W^*})$ disappears when the neutralino 4-momentum is added to the 4-momentum of the "b + 2 quarks$_W$" system.

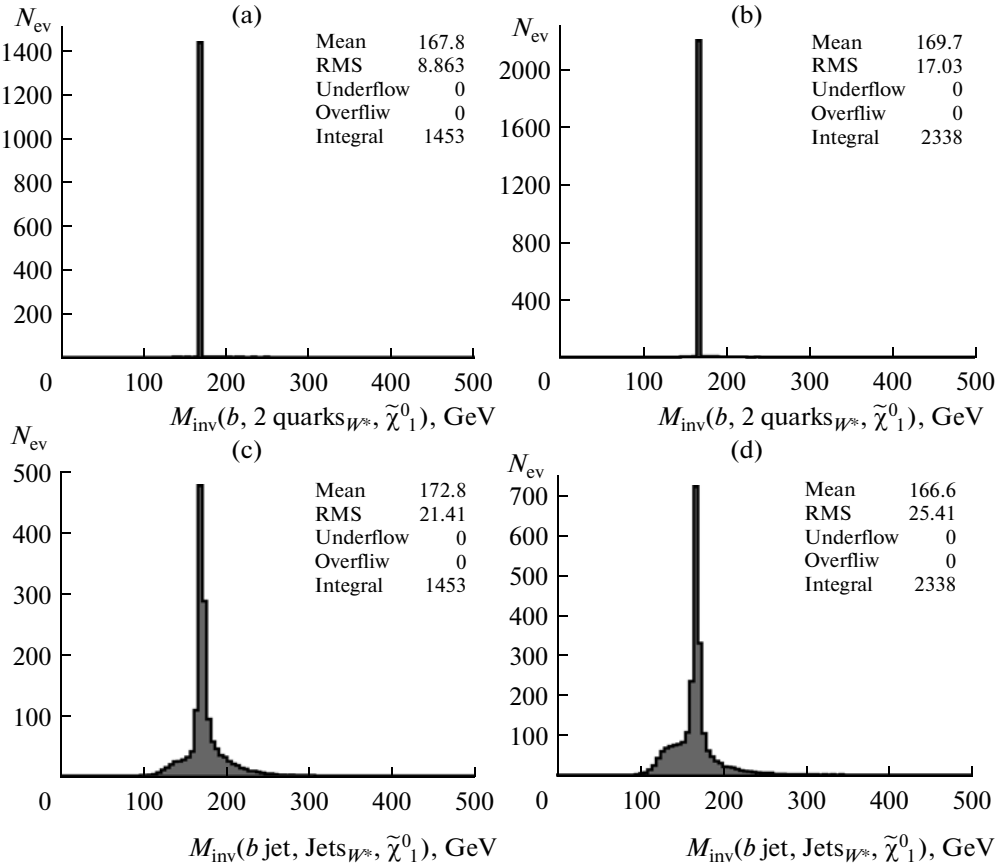

Fig. 21. The spectra of the invariant masses M_{inv} (b quark, 2 quarks$_{W^*}$, $\tilde{\chi}^0_1$) and M_{inv} (b jet, Jets$_W$, $\tilde{\chi}^0_1$). Plots (a)and (b) are for quarks level; plots (c)and (d) are for jets level. (a, c) "+−" and "−+" polarizations; (b, d) "++" and "− −" polarizations.

The influence of the effect of the hadronization of the b quarks and of the quarks from W decay into jets is shown in the plots c and d of Fig. 21. These plots demonstrate that the hadronization of quarks into jets practically does not change the positions of the stop mass peak, which practically coincides with the input value $M_{\tilde{t}_1} = 167.9$ GeV. It is also seen that the hadronization results in the appearance of more or less symmetrical and rather suppressed short tails around the peak position. The mean values of the distributions in the plots c and d of Fig. 21 are slightly different from the mean values of the quark level distributions shown in the plots a and b of Fig. 18, but the peak positions remain the same. It is easy to see from the plots c and d of Fig. 19 that, adding the mass of the neutralino $M_{\tilde{\chi}^0_1} = 80.9$ GeV to the value of the right edge point of the peak $M_{\text{inv}}(b\,\text{jet}, \text{Jets}_{W^*}) \approx 85.2$ GeV, one can get the left lower limit for the reconstructed stop mass $M^{\text{reco-low}}_{\tilde{t}_1} \approx 166.2$ GeV which reproduces well the input value $M_{\tilde{t}_1} = 167.9$ GeV.

Taking into account the bin width of 5 GeV used in the invariant mass distributions, we may conclude that the method of the stop mass reconstruction based on the peak positions will be quite useful.

CONCLUSIONS

We have studied stop pair production in photon–photon collisions within the framework of the MSSM for the total energy of the e^-e^- system $E^{\text{tot}}_{e^-e^-} = \sqrt{s_{ee}} = 1000$ GeV. We assume that the stop quark decays dominantly into a chargino and a b quark, $\tilde{t}_1 \to b\tilde{\chi}^{\pm}_1$, and the chargino decays into a neutralino and a W boson, $\tilde{\chi}^{\pm}_1 \to \tilde{\chi}^0_1 W^{\pm}$, where the W boson is virtual. One of the two W's decays hadronically, $W^+ \to q\bar{q}$, the other one leptonically, $W^- \to \mu^-\nu$.

The study is based on a Monte Carlo simulation with two programs. First, we have used the program CIRCE2 which gives the luminosity and the energy spectrum of the colliding backscattered photon beams. The results of CIRCE2 are taken as input for PYTHIA6.4. This event generator is used to simulate stop ($M_{\tilde{t}_1} = 167.9$ GeV) pair production and decay as

well as top pair production being the main background.

Three cuts (5)–(7) have been proposed. The second (6) and the third (7) cut are the most important for the separation of the signal stop events from the background top events. They restrict the value of the invariant mass of all four jets (produced in $\gamma\gamma \to \tilde{t}_1\tilde{t}_1 \to b\bar{b}q_i\bar{q}_j\mu\nu_\mu\tilde{\chi}_1^0\tilde{\chi}_1^0$ process) and the value of the detected energy. This set of cuts leads to a signal-to-background ratio as large as $S/B = 60$ in the case of the "+−" and "−+" polarizations and $S/B = 123$ in the case of the "++" and "− −" polarizations. Thus, we expect about 1–2% admixture of top events to the stop signal.

We have shown that determining the end point of the peak in the distribution of the invariant mass M_{inv} (b jet, Jets_{W^*}) of the "b jet + two jets from W decay" system allows us to reconstruct the mass of the stop quark with a good accuracy based on the statistics of about two years running. For this the mass of $\tilde{\chi}_1^0$ has to be known.

In conclusion, we can say that the $\gamma\gamma$ channel is very well suited for the study of stop pair production.

ACKNOWLEDGMENTS

This work is supported by the JINR-BMBF project and by the "Fonds zur Förderung der wissenschaftlichen Forschung" (FWF) of Austria, project no. P18959-N16. The authors acknowledge support from EU under the MRTN-CT-2006-035505 and MRTN-CT-2004-503369 network programmes. A.B. was supported by the Spanish grants SAB 2006-0072, FPA 2005-01269 and FPA 2005-25348-E of the Ministero de Educacion y Ciencia.

REFERENCES

1. J. Ellis and S. Rudaz, Phys. Lett. B **128**, 248 (1983); G. Altarelli and R. Rückl, Phys. Lett. B **144**, 126 (1984).
2. *International Linear Collider. Reference Design Report*, Vol. 2: *Physics at the ILC,* Ed. by A. Djouadi et al. ILC-REPORT-2007-001 (2007); hep-ph/0709.1893; http://www.linearcollider.org/cms/?pid=1000025
3. B. Badelek et al., *TESLA Technical Design Report*, Part VI: Appendices, Ed. by V. Telnov (DESY, 2001), Ch. 1: "The Photon Collider at TESLA"; hep-ex0108012.
4. I. F. Ginzburg et al., Preprint INP 81-50 (Novosibirsk, 1981); JETP Lett. **34**, 491 (1982); Preprint INP No. 81-102 (Novosibirsk, 1981); Nucl. Instrum. Methods Phys. Res. **205**, 47 (1983).
5. C. Akerlof, "Using the SLC as a Photon Accelerator," Preprint UM HE No. 81-59. (Univ. of Michigan, 1981, unpublished).
6. I. F. Ginzburg et al., Preprint INP No. 82-160 (Novosibirsk, 1982); Nucl. Instrum. Methods Phys. Res. **219**, 5 (1984).
7. I. F. Ginzburg et al., Sov. J. Nucl. Phys. **38**, 372 (1983).
8. I. F. Ginzburg et al., Sov. J. Nucl. Phys. **38**, 1021 (1983).
9. V. I. Telnov, Nucl. Instrum. Methods Phys. Res. A **294**, 72 (1990); Nucl. Instrum. Methods Phys. Res. A **355**, 3 (1995).
10. I. F. Ginzburg, Nucl. Instrum. Methods Phys. Res. A **355**, 63 (1995).
11. A. Bartl et al., Eur. Phys. J. C **2**, 6 (2000); hep-ph0002115.
12. M. Carena et al., Phys. Rev. D: Part. Fields **72**, 115008 (2005); hep-ph/0508152.
13. A. Bartl et al., "Stop Pair Production in Polarized Photon-Photon Collisions," in *Proceedings of the International Conference on Linear Colliders (LCWS 2004), April 19–23, 2004* (Le Carre des Sciences, Paris, 2004), Vol. II, p. 919.
14. A. Bartl et al., "On Pair Production of Scalar Top Quarks in $e^+ e^-$ Collisions at ILC and a Possibility of Their Mass Reconstruction," Part. Nucl. Lett **6**, 300–311 (2009); ILC-NOTE-2007-036; hep-ph/0906.3805.
15. A. Bartl et al., Pair Production of Scalar Top Quarks in Polarized Photon-Photon Collisions at ILC," ILC-NOTE-2007-036; hep-ph/0804.1700v3 (2010).
16. T. Sjostrand et al., Comput. Phys. Commun. **135**, 238 (2001).
17. T. Ohl, http://theorie.physik.uni-wuersburg.de/~ohl/circe2/cicre2.ps; http://theorie/physik/uni-wuerzburg.de/~ohl/circe2/manual004.html.
18. I. F. Ginzburg and V. G. Serbo, in *Proceedings of the 23rd Winter School of LINP* (1988), vol. 2, p. 132.
19. I. F. Ginzburg, "Physical Potential of Photon-Photon and Electron-Photon Colliders in TeV Region," in *Proceedings of the IX International Workshop on Photon-Photon Collisions* (San Diego, CA, USA, 1992), p. 474.
20. S. Berge, "Gluino and Squark Pair Production at Future Linear Colliders," DESY-THESIS-2003-048 (2003).
21. S. Berge, M. Klasen, and Y. Umeda, Phys. Rev. D: Part. Fields **63**, 035003 (2001).
22. E. Brubaker et al., hep-ex/0703034.
23. K. Yokoya and P. Chen, "Beam-Beam Phenomena in Linear Colliders," KEK Preprint No. 91-2 (1991).
24. V. I. Telnov, hep-ph/001201.
25. T. Takahashi et al., in *Proceedings of Snowmass Workshop* (1996).
26. P. Chen et al., Nucl. Instrum. Methods Phys. Res. A **397**, 458 (1997); physics/9704012.
27. G. Klamke and K. Moenig, Eur. Phys. J. C **42**, 261 (2005); DESY-05-049 (2005); hep-ph/0503191.
28. R. Hawkings, "Vertex Detector and Flavour Tagging Studies for TESLA Linear Collider," LC-PHSM-2000-021 (2000).
29. C. J. S. Damerell and D. J. Jackson, eConf960625. DET078 (1996); R. Hawkings, LC-PHSM-2000-021 (2000); S. M. Xella Hansen et al., LC-PHSM-2001-024 (2001); S. M. Xella Hansen et al., LC-PHSM-2003-061 (2003); S. M. Xella Hansen et al. (Linear Collider Flavour Identification Collab.), Nucl. Instrum. Methods Phys. Res. A **501**, 106 (2003).